Transport of N -acetylchitooligosaccharides and fluorescent N-acetylchitooligosaccharide analogs into rat liver lysosomes

Younès Bouzidi, Michaël Bosco, Haifei Gao, Stéphanie Pradeau, Lucrèce Matheron, Isabelle Chantret, Patricia Busca, Sébastien Fort, Christine Gravier-Pelletier, Stuart Moore

▶ **To cite this version:**

Younès Bouzidi, Michaël Bosco, Haifei Gao, Stéphanie Pradeau, Lucrèce Matheron, et al.. Transport of N -acetylchitooligosaccharides and fluorescent N-acetylchitooligosaccharide analogs into rat liver lysosomes. Glycobiology, 2024, 34 (2), pp.cwad099. 10.1093/glycob/cwad099 . hal-04601870

HAL Id: hal-04601870
https://hal.science/hal-04601870

Submitted on 5 Jun 2024

HAL is a multi-disciplinary open access archive for the deposit and dissemination of scientific research documents, whether they are published or not. The documents may come from teaching and research institutions in France or abroad, or from public or private research centers.

L'archive ouverte pluridisciplinaire **HAL**, est destinée au dépôt et à la diffusion de documents scientifiques de niveau recherche, publiés ou non, émanant des établissements d'enseignement et de recherche français ou étrangers, des laboratoires publics ou privés.

Transport of *N*-acetylchitooligosaccharides and fluorescent *N*-acetylchitooligosaccharide analogs into rat liver lysosomes

Younès Bouzidi[1,†], Michaël Bosco[2,†], Haifei Gao[2], Stéphanie Pradeau[3], Lucrèce Matheron[4], Isabelle Chantret[1], Patricia Busca[2], Sébastien Fort[3], Christine Gravier-Pelletier[2], Stuart E.H. Moore[1,*]

[1]INSERM U1149, Université Paris Cité, 16 rue Henri Huchard, Paris 75018, France, [2]CNRS UMR8601, Université Paris Cité, 45 rue des Saints Pères, Paris 75006, France, [3]CNRS, CERMAV, Université Grenoble Alpes, 601 Rue de la Chimie, 38610 Gières, France, [4]Plateforme MS3U, Fédération de chimie moléculaire Paris centre FR2769, Sorbonne Université, 4 place Jussieu, Paris 75005, France

*Corresponding author: INSERM U1149, Faculté de Medicine Xavier Bichat, Université Paris Cité, 16 rue Henri Huchard, Paris 75018 France.
Email: stuart.moore@inserm.fr

†Younès Bouzidi and Michaël Bosco contributed equally

Free polymannose-type oligosaccharides (fOS) are processed by cytosolic enzymes to generate $Man_5GlcNAc$ which is transferred to lysosomes and degraded. Lysosomal fOS import was demonstrated in vitro but is poorly characterized in part due to lack of convenient substrates. As chitooligosaccharides (COS, oligomers β1,4-linked GlcNAc) block [^{3}H]$Man_5GlcNAc$ transport into lysosomes, we asked if COS are themselves transported and if so, can they be chemically modified to generate fluorescent substrates.

We show that COS are degraded by lysosomal hydrolases to generate GlcNAc, and robust ATP-dependent transport of [^{3}H]COS2/4 di and tetrasaccharides into intact rat liver lysosomes was observed only after blocking lysosomal [^{3}H]GlcNAc efflux with cytochalasin B. As oligosaccharides with unmodified reducing termini are the most efficient inhibitors of [^{3}H]COS2/4 and [^{3}H]$Man_5GlcNAc$ transport, the non-reducing GlcNAc residue of COS2-4 was de-*N*-acetylated using *Sinorhizobium meliloti* NodB, and the resulting amine substituted with rhodamine B (RB) to yield RB-COS2-4. The fluorescent compounds inhibit [^{3}H]$Man_5GlcNAc$ transport and display temperature-sensitive, ATP-dependent transport into a sedimentable compartment that is ruptured with the lysosomotropic agent L-methyl methionine ester. Once in this compartment, RB-COS3 is converted to RB-COS2 further identifying it as the lysosomal compartment. RB-COS2/3 and [^{3}H]$Man_5GlcNAc$ transports are blocked similarly by competing sugars, and are partially inhibited by the vacuolar ATPase inhibitor bafilomycin and high concentrations of the P-type ATPase inhibitor orthovanadate.

These data show that $Man_5GlcNAc$, COS2/4 and RB-COS2/3 are transported into lysosomes by the same or closely related mechanism and demonstrate the utility of COS modified at their non-reducing terminus to study lysosomal oligosaccharide transport.

Key words: autophagy; lysosome; oligosaccharide; protein N-glycosylation; sugar transport.

Introduction

Autophagic pathways promote the recycling of unwanted material within the cell. The common end point of these processes is the lysosomal disassembly of complex structures into their composite building blocks, which are then exported into the cytosol for redeployment as required. Autophagy is initiated by several targeting and capture processes. Large components such as organelles, bacteria, viruses, and glycogen particles are engulfed by a membrane which fuses with the lysosome (Codogno et al. 2011). Some proteins are directly translocated from the cytosol to the lysosomal interior by ATP-dependent chaperone mediated autophagy (CMA) (Kaushik and Cuervo 2018). RNA and DNA fragments are transported into lysosomes by an ATP-dependent mechanism requiring Lamp2c and Sidt2 (Hase et al. 2020) and peptides are pumped into the lysosome by an ABC-type transporter (Abcb9/Tapl) (Demirel et al. 2010; Demirel et al. 2012). Regarding the transport of oligosaccharides, while the cytosol-to-lysosome transport of (free) polymannose type oligosaccharides (fOS) has been described (Saint-Pol et al. 1997; Moore 1999; Saint-Pol et al. 1999), the molecular origins of this process are still not known. It has been shown, *in vivo*, that fOS generated during protein *N*-glycosylation ($Man_{8\text{-}9}GlcNAc_2$) are trimmed by the cytosolic endoglucosaminidase (Engase1) and mannosidase (Man2c1p) to produce $Man_5GlcNAc$ (Pierce et al. 1979; Verbert and Cacan 1999; Suzuki et al. 2002; Suzuki et al. 2006; Chantret et al. 2010), which is subsequently transferred to lysosomes by a process that is not blocked by 3-methyladenine (3MA), a classical inhibitor of macroautophagic sequestration (Saint-Pol et al. 1997). Using rat liver lysosomes, *in vitro* experiments revealed saturable and ATP-dependent lysosomal import of [^{3}H]$Man_5GlcNAc$ (Saint-Pol et al. 1999). This lysosomal oligosaccharide transport (LOST) process was suggested to underlie the cytosol-to-lysosome transfer of fOS seen *in vivo*. However, [^{3}H]$Man_{4\text{-}3}GlcNAc$ oligosaccharides are better transport substrates than [^{3}H]$Man_5GlcNAc$ itself, and chitooligosaccharides (COS: linear chains of β1-4 linked residues of GlcNAc) containing 2, 3 or 4 residues of GlcNAc (COS2-4) inhibit the transport of [^{3}H]$Man_5GlcNAc$ into lysosomes with high efficiency (Saint-Pol et al. 1999), suggesting that LOST may also be involved in regulating other cytosolic oligosaccharides. Indeed, if the above-described scheme for fOS catabolism is correct, the rate limiting

step is the lysosomal sequestration of $Man_5GlcNAc$, which is the most abundant fOS found in mammalian cells at steady state (Iwai et al. 1999; Ohashi et al. 1999; Yanagida et al. 2006). Understanding the precise role of LOST in lysosomal physiology and oligosaccharide metabolism will require identification of LOST at the molecular level and its manipulation *in vivo* using genetic approaches. To this end, we are developing chemical tools for the assay, and characterization of LOST. COS are convenient starting materials for chemical syntheses (Chambon et al. 2017) and here, we report the transport of [^{3}H]COS2, [^{3}H]COS4 and fluorescently labeled COS analogs into lysosomes *in vitro*. The biochemical characteristics of the transport of these molecules into lysosomes are similar to those reported for lysosomal import of [^{3}H]$Man_5GlcNAc$, suggesting that the same, or closely related, mechanism is responsible.

Results

Only COS with less than 5 residues of GlcNAc inhibit lysosomal [^{3}H]M5 import optimally

LOST was initially identified *in vitro* by incubating intact rat liver lysosomes with a mixture of radioactive fOS (hereafter, called [^{3}H]M5) comprising predominantly [^{3}H]$Man_5GlcNAc$ (Saint-Pol et al. 1999, Fig. 1A). The mannosidase inhibitor swainsonine (SW) must be added to transport assay incubations otherwise [^{3}H]M5 is degraded and the resulting [^{3}H]mannose is exported into the incubation medium (Fig. 1A, right panel). LOST is ATP-dependent, and ATP and an ATP-regenerating system are added to transport assay mixtures. After incubating at 25 °C for 40 min, ice-cold buffered sucrose is added to stop the reactions, and after pelleting and washing the lysosome fraction, radioactivity associated with the final pellet is assayed by scintillation counting (Fig. 1A, left panel). Using this assay, it was shown that COS2-4 inhibit transport of [^{3}H]M5 into lysosomes (Fig. 1A, right panel) with similar potencies, and more efficiently than the Manβ1,4GlcNAc disaccharide that corresponds to the reducing terminus of $Man_5GlcNAc$ (Saint-Pol et al. 1999). Based on these findings, the optimal length of COS for transport inhibition was determined, and as shown in Fig. 1B, COS5 and COS6 are ~40- and ~500-fold less efficient, respectively, than COS4 at inhibiting transport. Accordingly, we focused on COS2-4 as potential LOST substrates.

Transport of [^{3}H]COS2 into lysosomes

COS2-4 are potentially degraded by both lysosomal β-hexosaminidase (β-Hex) and chitobiase (Ctbs) and possibly a third enzyme (Persichetti et al. 2012) to yield GlcNAc, which could then be exported by the lysosomal HexNAc transporter (Fig. 1C) (Jonas et al. 1989; Jonas and Jobe 1990). Although potent membrane permeant β-Hex inhibitors like PUGNAc (*O*-(2-acetamido-2-deoxy-d-glucopyranosylidene)amino-*N*-phenylcarbamate) are available (Macauley and Vocadlo 2010) that, at concentrations up to 1 mM, do not inhibit transport of [^{3}H]M5 into lysosomes (Supplementary Fig. 1A), there are no known membrane permeant Ctbs inhibitors. When [^{3}H]COS2 was incubated with lysosomes in either the absence or presence of ATP, robust ATP-dependent

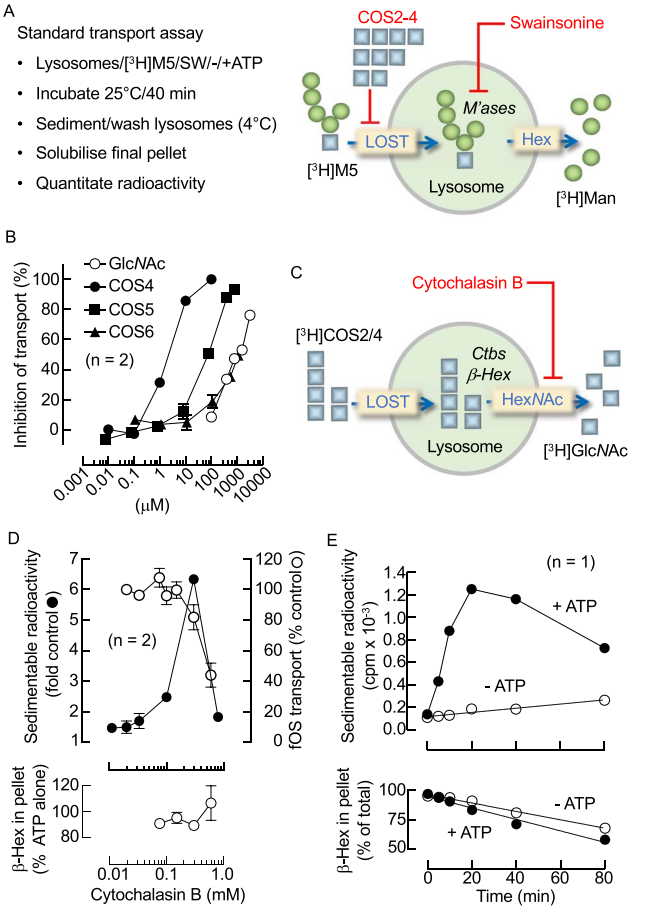

Fig. 1. Inhibition of [^{3}H]M5 transport by COS and development of strategy for measuring [^{3}H]COS2 transport into rat liver lysosomes. A) The different steps of the standard transport assay using the [^{3}H]M5 substrate are indicated in the left panel. As shown in the right panel, without the addition of swainsonine (SW), which inhibits lysosomal mannosidases (*M'ases*), [^{3}H]mannose (spheres) released from [^{3}H]M5 is rapidly exported from the lysosome into the incubation medium (see also the upper panel of Supplementary Fig. 1C). COS2-4, comprising linear chains of GlcNAc (squares) block entry of [^{3}H]M5 into the lysosome (Saint-Pol et al. 1999). B) Standard [^{3}H]M5 transport assays were carried out in the presence of increasing concentrations of the indicated COS. Inhibition of the ATP-dependent transport is expressed as a percentage of transport seen in the absence of competitor. C) COS2/4 are potentially transported into lysosomes by LOST, and after hydrolysis by lysosomal hydrolases such as β-hexosaminidase (*β-Hex*) and chitobiase (*Ctbs*), the resulting residues of GlcNAc could be rapidly exported into the incubation medium by a previously described GlcNAc/Gal*N*Ac transporter (Hex*N*AcT) (Jonas et al. 1989). D) [^{3}H]COS2 was incubated with lysosomes and ATP in the presence of the indicated concentrations of CytB for 40 min at 25 °C. At the end of the incubation, lysosomes were washed in the presence of CytB at 4 °C, and radioactivity associated with the final pellet was quantitated (upper panel, solid symbols). Under the same conditions, the effect of CytB on [^{3}H]$Man_5GlcNAc$ transport was measured (upper panel, open symbols). β-Hexosaminidase (β-Hex) was measured in the pellets and the activity is expressed as a percentage of that found in the presence of ATP alone (lower panel). E) Lysosomes were incubated with [^{3}H]COS2 and 300 μM CytB in either the absence or presence of ATP for the indicated times. After washing the lysosomes, radioactivity associated with pellets was assayed (upper panel). β-Hex was measured in both the pellets and supernatants and the activity remaining in the pellets is expressed as a percentage of total activity (lower panel).

increases in sedimentable radioactivity were not detected even in the presence of PUGNAc (Supplementary Fig. 1B). Nevertheless, when whole transport assay reaction mixtures were analyzed without separation of lysosomes from the reaction medium (Supplementary Fig. 2A), Biogel P2 size exclusion chromatography (SEC) revealed an ATP-dependent production of [^{3}H]GlcNAc (Supplementary Fig. 2B). This suggested that in the presence of ATP either [^{3}H]COS2 is degraded in lysosomes and the resulting [^{3}H]GlcNAc is rapidly returned to the incubation medium, or [^{3}H]COS2 hydrolysis occurs in the incubation medium itself. To examine this issue, experiments to trap any [^{3}H]GlcNAc potentially produced within lysosomes were undertaken. The lysosomal Hex*N*Ac transporter is inhibited by cytochalasin B (CytB) (Jonas et al. 1989), and as shown in the upper panel of Fig. 1D, 30–300 μM CytB, increases sedimentable radioactivity when lysosomes are incubated with [^{3}H]COS2 and ATP, but at higher concentrations, this effect is abolished. The reduced sedimentable radioactivity observed at the higher CytB concentrations is not associated with a reduction in lysosomal integrity, as measured by sedimentable β-Hex (Fig. 1D, lower panel), but correlates with an inhibition of [^{3}H]Man$_5$GlcNAc transport (Fig. 1D, upper panel). Transport assays conducted in the presence of 300 μM CytB, with or without ATP are shown in Fig. 1E and an ATP-dependent increase in sedimentable radioactivity is seen over the first 20 min followed by a slow decline. The origin of this decline could be accounted for by the fact that 300 μM CytB is insufficient for complete trapping of [^{3}H]GlcNAc in the lysosome, therefore at later incubation times when the rate of [^{3}H]COS2 import is potentially slowing there is a net efflux of radioactivity via the HexNAc transporter. Alternatively, at later incubation times, reduced lysosomal integrity (Fig. 1D, lower panel) may also contribute to the net efflux of [^{3}H]GlcNAc. Next, transport mixtures were centrifuged and the pellets as well as the supernatants were analyzed by SEC as shown in Fig. 2A. As expected, in the absence of CytB, 98% of the ATP-dependent [^{3}H]GlcNAc is recovered in the supernatant fraction (Fig. 2A; lower right panel, Fig. 2B). In the presence of CytB, only 45% of total ATP-dependent [^{3}H]GlcNAc is recovered from the supernatant (Fig. 2A; lower right panel, Fig. 2B) and there is an 18.5-fold increase in [^{3}H]GlcNAc associated with the pellet (Fig. 2A; upper right panel, Fig. 2B). Quantitation of the [^{3}H]GlcNAc associated with both the pellets and supernatants indicates that CytB reduces total ATP-dependent [^{3}H]GlcNAc production by 17%. This would be anticipated if [^{3}H]COS2 enters the lysosome via LOST, which is inhibited ~20% by 300 μM CytB (see Fig. 1D, upper panel). Although CytB only partially inhibits the appearance of [^{3}H]GlcNAc in the supernatant fraction, the ensemble of this data supports the hypothesis that [^{3}H]COS2 is transported into lysosomes where it is hydrolyzed to generate [^{3}H]GlcNAc, which is then rapidly returned to the incubation medium (Fig. 2C).

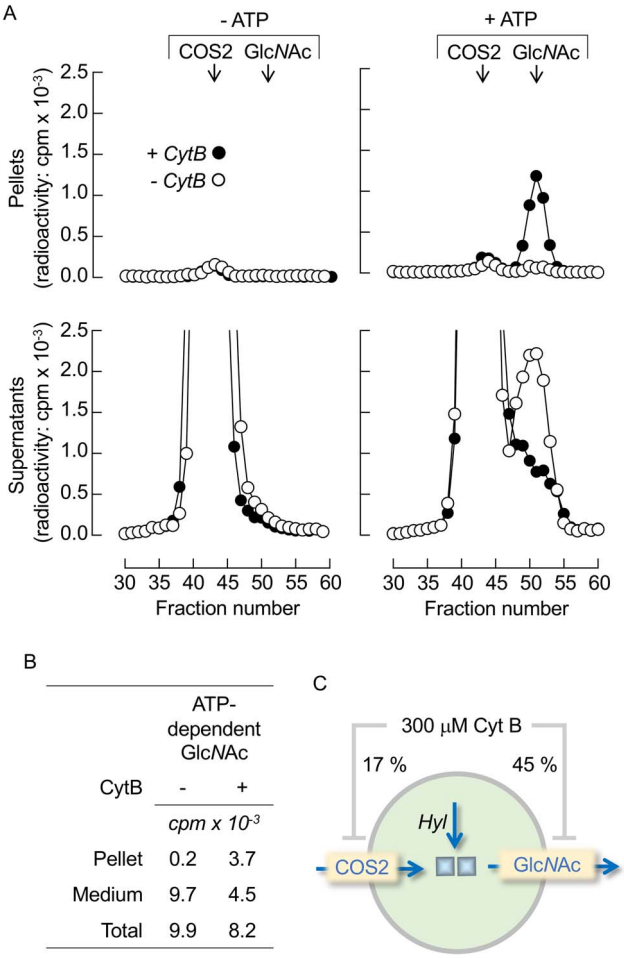

Fig. 2. Cytochalasin B provokes the appearance of sedimentable [^{3}H]GlcNAc during incubation of lysosomes with [^{3}H]COS2. A) [^{3}H]COS2 was incubated with lysosomes in either the absence (left panels) and presence (right panels) of ATP, and the absence (open symbols), or presence of 300 μM cytochalasin B (CytB, solid symbols) for 20 min at 25 °C. Lysosomes were washed as described for Fig. 1, and water-soluble material recovered from the pellets (upper panels) and supernatants (lower panels) was subjected to Biogel P2 size exclusion chromatography as described in materials and methods. The elution positions of standard [^{3}H]COS2 and [^{3}H]GlcNAc are indicated. B) Radioactivity associated with the [^{3}H]COS2 and [^{3}H]GlcNAc peaks observed in the experiment shown in A was quantitated and after subtracting values found in the absence of ATP from those obtained in the presence of ATP, ATP-dependent [^{3}H]GlcNAc was computed for both the pellet and supernatant fractions. C) As described in the text, the data are compatible with the indicated scheme where CytB differentially inhibits lysosomal import of [^{3}H]COS2 and, after hydrolysis by lysosomal hydrolases (*Hyl*), export of [^{3}H]GlcNAc.

[^{3}H]COS2 and [^{3}H]COS4 transport is saturable and has similar selectivity to [^{3}H]Man$_5$GlcNAc transport

Using the CytB-based transport assay it was shown that [^{3}H]COS2 and [^{3}H]COS4 transport demonstrate similar saturable kinetics (Fig. 3A), although [^{3}H]COS4 transport has a 1.5-fold higher apparent K_{uptake} and 20% reduction in maximal transport rate compared to [^{3}H]COS2 transport. If [^{3}H]COS are transported into lysosomes by LOST, the CytB- and ATP-dependent increases in sedimentable radioactivity should be reduced by oligosaccharides that are known to inhibit LOST-mediated transport of [^{3}H]M5. All potential competitors were used at a concentration of 10 μM because at this concentration of COS2, about 50% inhibition of [^{3}H]M5 transport is observed. First, the rank orders of inhibitory potency of the competitors is the same for [^{3}H]COS2, [^{3}H]COS4 and [^{3}H]M5 transport (Fig. 3B). Second, [^{3}H]COS2 and [^{3}H]COS4 transport are more sensitive to the compounds than [^{3}H]M5 transport (Fig. 3B). This could be explained by the potentially lower specific activity of [^{3}H]M5 preparation compared to those of the [^{3}H]COS2 (1.6 Ci/mmol) and [^{3}H]COS4 (1 Ci/mmol)

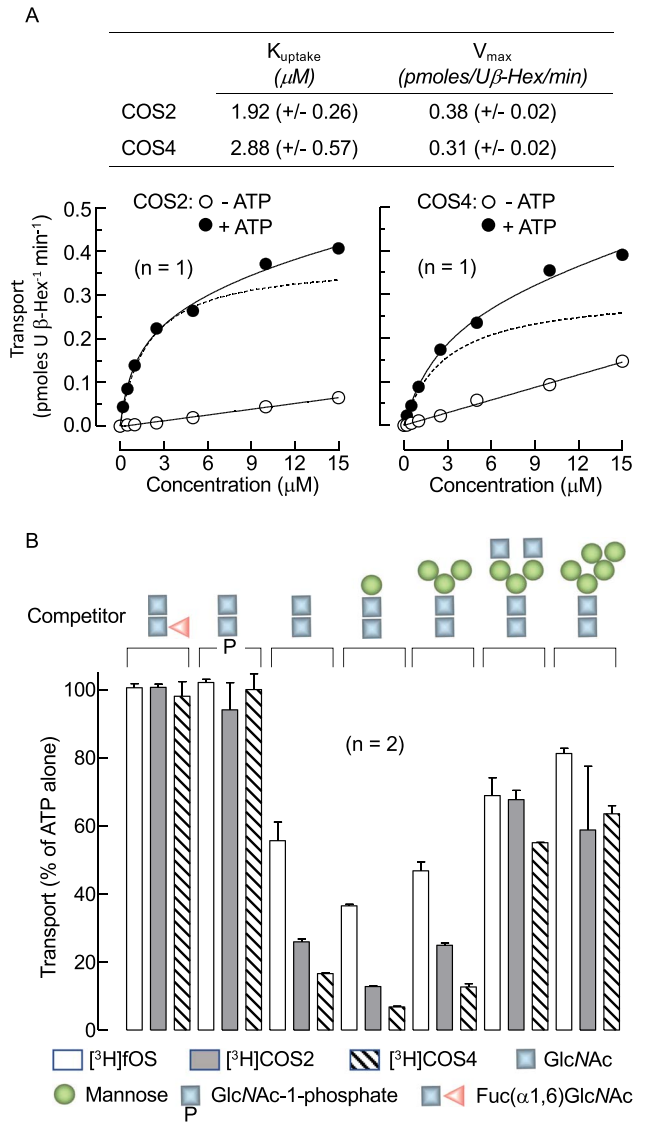

	K_{uptake} (μM)	V_{max} (pmoles/Uβ-Hex/min)
COS2	1.92 (+/- 0.26)	0.38 (+/- 0.02)
COS4	2.88 (+/- 0.57)	0.31 (+/- 0.02)

Fig. 3. Characteristics of [^{3}H]COS2, [^{3}H]COS4 and [^{3}H]M5 transport into lysosomes. A) Increasing amounts of [^{3}H]COS2 and [^{3}H]COS4 were incubated with lysosomes under the standard [^{3}H]COS transport assay conditions. After measuring the amount of β-Hex present in the incubations, the apparent transport constants K_{uptake} and V_{max} (+/− SD) were calculated using the GraphPad prism 5 Michaelis-Menten analysis of the ATP-dependent transport data sets (dotted lines). B) Standard [^{3}H]COS2/4 and [^{3}H]M5 transport assays were carried out in the presence of the indicated compounds at a final concentration of 10 μM. The bars represent the reduction in transport expressed as a percentage of the transport seen in the presence of ATP alone.

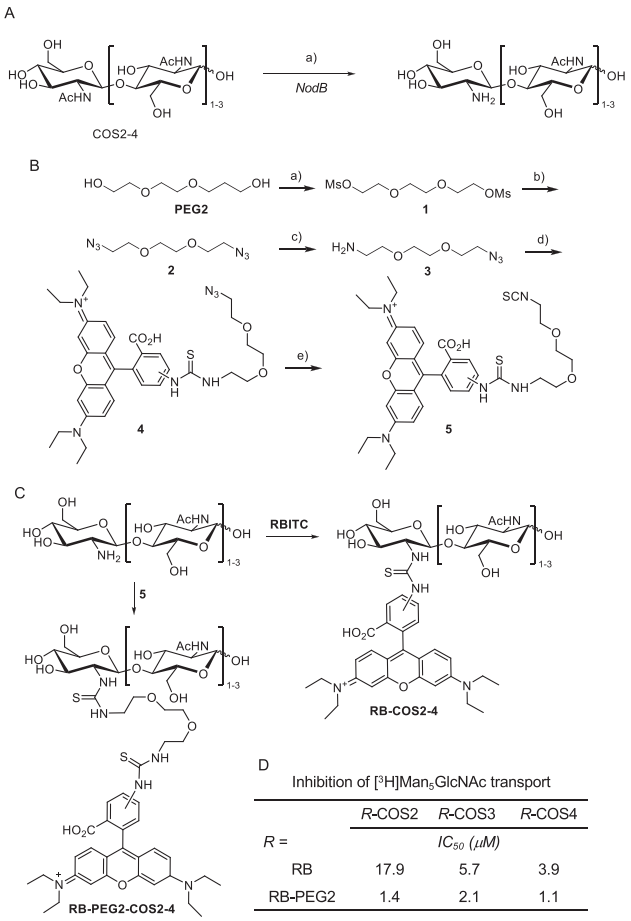

D Inhibition of [^{3}H]Man$_5$GlcNAc transport

R =	R-COS2	R-COS3	R-COS4
	IC_{50} (μM)		
RB	17.9	5.7	3.9
RB-PEG2	1.4	2.1	1.1

Fig. 4. Synthesis and biological testing of rhodamine labeled COS-based probes. Reagents and conditions: A. a) *S. Meliloti* NodB chitinoligosaccharide *N*-deacetylase, 20 mM MOPS pH 7.2 containing 10 mM DTT and 1 mM $MnSO_4$ during 20 h at 30 °C, total conversion (isolated yields COS4 84%, COS3 56%, COS2 50%). B. a) MsCl, Et_3N, CH_2Cl_2, 0 °C to r.t., 16 h; b) NaN_3, DMF, 60 °C, 72 h; c) PPh_3, Et_2O, THF, HCl aq. 1 M, r.t., 16 h; d) RBITC, DMSO, r.t.; e) PPh_3, CS_2, THF, r.t., 16 h. C. RBITC or isothiocyanate **5**, DMSO, 60 °C, 16 h to 96 h, 19% to 45%. D) The ability of the indicated fluorescent compounds to inhibit [^{3}H]M5 transport into lysosomes was assessed, as described in Fig. 1A, and the IC_{50} values are reported.

substrates. More particularly, none of the transport processes were significantly inhibited, at this concentration, by sugars whose reducing *N*-acetylglucosamine residue is modified by either a phosphate at position C1 or an α1,6-linked fucose residue. Also, the larger oligosaccharides, $Man_5GlcNAc_2$ and $GlcNAc_2Man_3GlcNAc_2$ are less effective at blocking the two transport processes than the smaller ($Man_{1-3}GlcNAc_2$) compounds. These data indicate that the [^{3}H]COS2, [^{3}H]COS4 and [^{3}H]M5 transport processes have similar selectivities.

Synthesis of fluorescent COS-based probes

Data presented in Fig. 3B suggest that substitution of the reducing end of COS with fluorophores will yield poor transport substrates. On the other hand, the similar capacities of $Man_{3\text{-}0}GlcNAc_2$ compounds to inhibit COS transport suggests that modification of the non-reducing end of chitobiose with fluorophores could potentially have less deleterious consequences. To achieve this the non-reducing GlcNAc residue of COS2-4 are de-*N*-acetylated enzymatically (Fig. 4A), allowing condensation of the amine of the non-reducing sugar with either rhodamine B (RB) isothiocyanate, or, via a PEG2 linker to potentially optimize the recognition of LOST, RB-PEG2-isothiocyanate (Fig. 4B).

RB- and RB-PEG2-COS analogs inhibit [^{3}H]M5 transport into lysosomes

The fluorescent probes shown in Fig. 4C were tested for their capacity to inhibit transport into lysosomes. RB-COS2 inhibited [^{3}H]M5 transport somewhat less efficiently than COS2-4 (IC_{50} 5–10 μM, see Fig. 1A (Saint-Pol et al. 1999)), but the addition of the PEG2 linker (RB-PEG2-COS2) between the sugar and the fluorophore increased [^{3}H]M5 transport inhibition efficiency over 10-fold (Fig. 4D). Whereas RB-COS3 and

RB-COS4 are less potent than RB-COS2, RB-PEG2-COS3 and RB-PEG2-COS4 demonstrated similar potency to that of RB-PEG2-COS2. Generally, the RB-PEG2 analogs have lower IC_{50} values than their corresponding starting COS. These data reveal a complex relationship between the structure of the fluorescent COS analogs and their capacity to inhibit [^{3}H]M5 transport: the PEG2 spacer and length of the COS both playing important roles.

ATP-dependent association of fluorescent COS analogs with an L-methyl methionine ester sensitive compartment

Next, an assay procedure was developed to specifically detect transport of fluorescent probes into lysosomes. Association of fluorescence with sedimentable membranes could be due to binding of probes to the cytoplasmic face of lysosomes or other organelles such as mitochondria and peroxisomes that are known to contaminate the lysosome preparation used here. To distinguish between these possibilities, lysosomes were selectively lysed using L-methyl methionine ester (L-meM). Incubation of lysosomes with this reagent, but not the non-hydrolyzable isomer, D-methyl methionine ester (D-meM) causes lysosome rupture without affecting mitochondria or peroxisomes (Goldman 1976; Reeves 1979; Reeves and Reames 1981). It is thought that while both compounds freely diffuse across the lysosome membrane, only the former is hydrolyzed by lysosomal esterases to yield methionine. Methionine does not easily diffuse across the membrane, and, at low temperature, its carrier-mediated efflux is too slow to protect the lysosome from osmotic lysis (Goldman 1976; Reeves 1979; Reeves and Reames 1981). Practically, as shown in Fig. 5A, after transport incubations, sedimentable material was washed with sucrose/HEPES buffer (SH) to remove unincorporated probe and divided into two aliquots, to which equal volumes of either 2.5 mM L-meM or 2.5 mM D-meM in SH are added. After 15 min on ice and centrifugation, the supernatants are recovered, and fluorescence is measured. Transport incubations in the absence or presence of RB-COS3 were conducted (Fig. 5B), and it was confirmed that L-, but not D-meM provoked release of lysosomal acid phosphatase (AP) from transport pellets even when the preceding transport incubations were conducted in the absence of ATP (Fig. 5B, upper panel). The fluorescence of the D-meM lysates was low in both the absence (Fig. 5B, middle panel) or presence (Fig. 5B, lower panel) of probe and was independent of either the temperature or the absence/presence of ATP in the preceding transport incubations. By contrast, the L-meM lysates revealed a temperature- and ATP-dependent increase in fluorescence when the probe was present in the transport assay mix (Fig. 5B, middle and lower panels). Accordingly, subtraction of the D-meM supernatant fluorescence values from their L-meM counterparts is taken to give an estimate of probe transport into the L-meM-sensitive compartment.

Next, using this approach, transport of the different RB-COS analogs into the L-meM-sensitive compartment was evaluated. First, the role of COS length was investigated (Fig. 5C). The di-, tri and tetrasaccharide-based compounds demonstrate an ATP-dependent signal but only the RB-COS2 and RB-COS3 signals were efficiently blocked by the COS2 competitor. Second, in different experiments, it is shown that linkage of the fluorophore to the sugar with a PEG2 spacer strikingly reduced the signal for both the COS2- (Fig. 5D) and

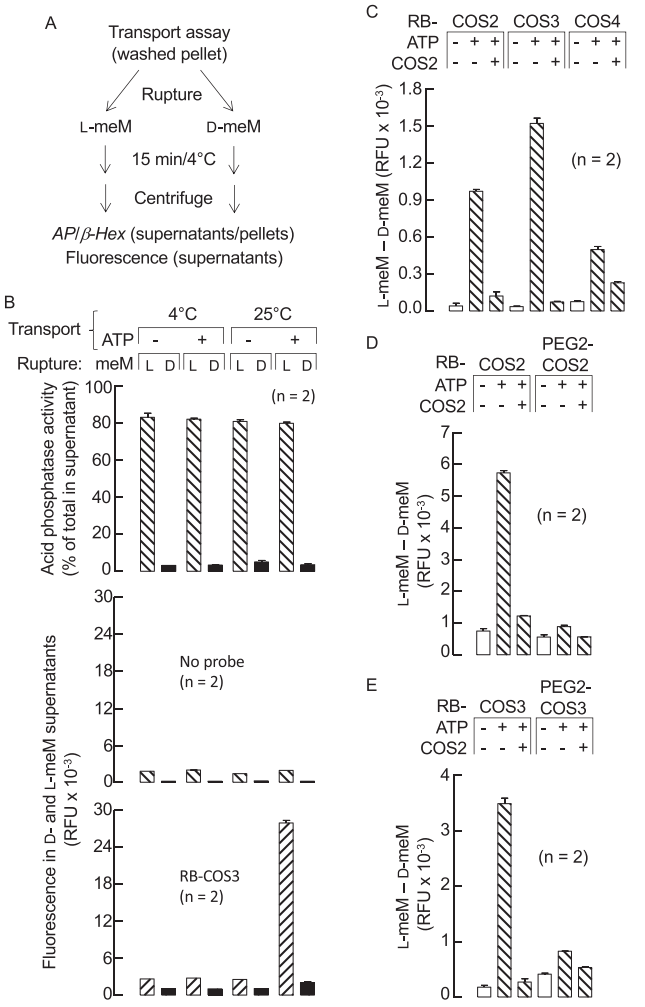

Fig. 5. Transport assay for fluorescent COS-based analogs. A) Protocol for detection of fluorescent compounds inside lysosomes using D- and L-methyl methionine esters (D-, L-meM). B) Transport assays were conducted in the absence (upper and middle panels) or presence of 20 μM RB-COS3 (lower panel) under the indicated transport conditions. After treatment of the washed transport pellets with D- and L-meM esters as shown in A, acid phosphatase activity was measured in the lysates and pellets (upper panel, data obtained using transport incubations conducted in the absence of fluorescent probe). The fluorescence associated with the D- and L-meM lysates is shown in the middle (no probe) and lower (RB-COS3) panels. C–E) Comparison of transport signals for the different fluorescent probes in three experiments using different lysosome preparations: (C) incubation of 20 μM RB-COS2-4 with lysosomes in the absence or presence of ATP and 4 mM COS2, (D) incubation of 20 μM RB-COS2 and RB-PEG2-COS2 with lysosomes in the absence or presence of ATP and 4 mM COS2, (E) 20 μM RB-COS3 and RB-PEG2-COS3 were incubated with lysosomes in the absence or presence of ATP and 4 mM COS2. After washing lysosomes and treatment with D- and L-meM esters, the fluorescence associated with the D-meM lysate was subtracted from that of the L-meM lysate to yield the transport signal as described in the text.

COS3-based (Fig. 5E) compounds. The RB-COS2 and RB-COS3 signals suggested that these compounds are potentially the most promising probes.

Conversion of RB-COS3 to RB-COS2 within the L-meM-sensitive compartment

The release of fluorescence from sedimentable material by L-, but not D-meM indicates that the fluorescent probes are

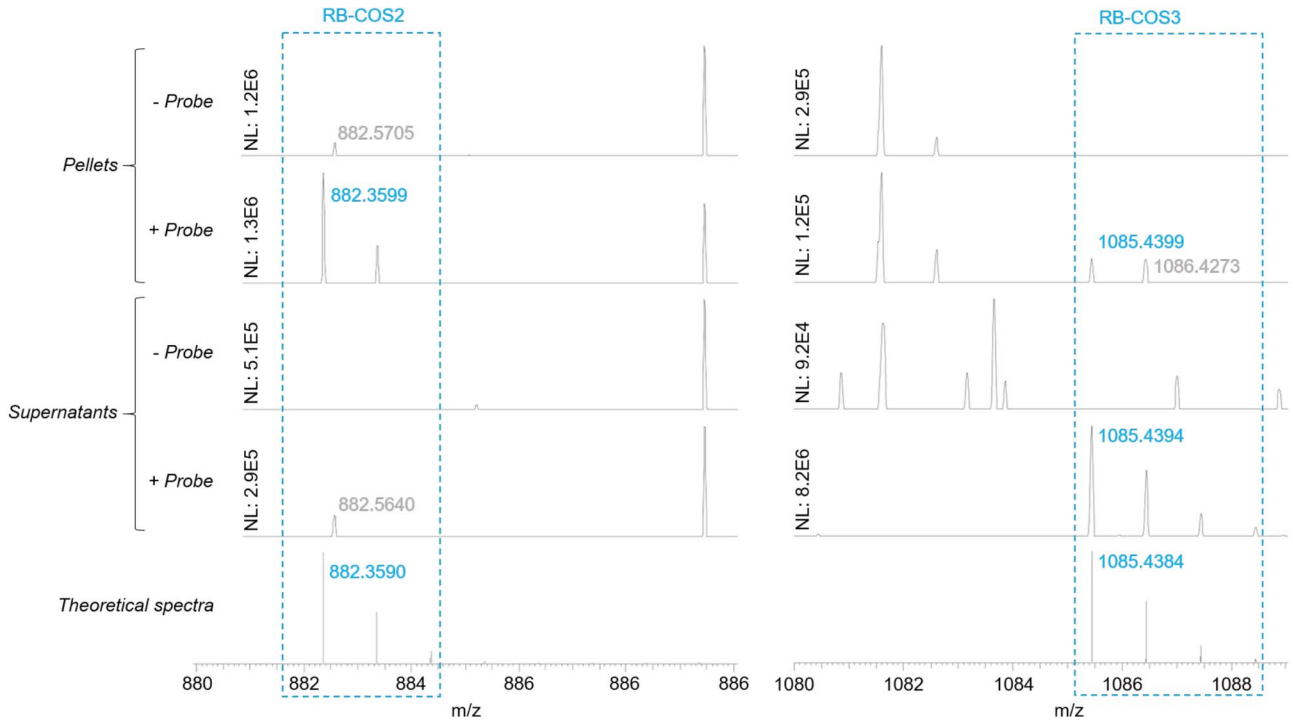

Fig. 6. Mass spectrometry of probes recovered from a standard RB-COS3 transport assay. Fluorescent probes were extracted from both the RB-COS3 transport supernatant (*supernatants*) and L-meM lysate of the washed transport pellet (*pellets*) as described in materials and methods. In parallel, to the RB-COS3 transport incubation (+*probe*) a transport incubation conducted in the absence of probe (−*probe*) was processed in the same way to give background spectra. ESI-HRMS was performed as described in materials and methods, and the RB-COS2 and RB-COS3 regions of the spectra are shown. Normalized level (NL) scales have been varied to better see how much more intense the RB-COS3 ions are in *supernatant + probe*, and to better realize when a signal is not much more than noise. Sodium adducts were also identified for the RB-COS3 ion in the *supernatant + probe* condition but are not shown.

transported into lysosomes. To further establish this point, we asked if the fluorescent material released from organelles by L-meM had been acted on by hydrolases within lysosomes. Because the non-reducing GlcNAc moiety of RB-COS probes are modified, these compounds are not expected to be hydrolyzed by lysosomal β-Hex, chitotriosidase (Cht1) or acid chitinase (AMCase), which are non-reducing end glycosidases (van Eijk et al. 2005; Kimura et al. 2019). By contrast, lysosomal Ctbs is a reducing end exoglycosidase that requires its substrates to have at least two intact β1,4-linked residues of GlcNAc (Aronson et al. 1989; Aronson and Halloran 2006), so, while not predicted to act on RB-COS2, this enzyme potentially converts RB-COS3 to RB-COS2. When incubated with lysosomal extracts at pH 4.5 at 25 °C for 3 h, mass spectrometric analyses of the recovered probe revealed conversion of RB-COS3 to RB-COS2 (Supplementary Fig. 3A), whereas ions corresponding to RB-GlcNAc or its degradation product RB-GlcNAc thiazoline were not detected when RB-COS2 was incubated under the same conditions (Supplementary Fig. 3B). Next, after a standard RB-COS3 transport assay, probe was extracted from both the transport incubation medium after pelleting of organelles, and from the L-meM lysate of the washed pellet. Mass spectrometric analysis revealed signals expected of RB-COS2 in the L-meM lysate but not in the transport incubation medium (Fig. 6). RB-COS3 was difficult to detect in the L-meM lysate, suggesting that after transport into the L-meM compartment it is rapidly hydrolyzed. These data show that the L-meM-sensitive compartment contains an activity characteristic of lysosomal Ctbs, further confirming that RB-COS probes are transported into the lysosome.

Apparent kinetics and selectivity of RB-COS2/3 transport into lysosomes

The apparent kinetic parameters of RB-COS2/3 transports are shown in Fig. 7A. RB-COS3 displays an apparent K_{uptake} that is 6.9-fold lower than that of RB-COS2, but RB-COS2 has a 3.8-fold higher apparent V_{max} than the COS3-based compound. Next, the capacity of COS2 and COS2ol and GlcNAc to quench transport of RB-COS probes into lysosomes was examined in more detail. Data shown in Fig. 7B show that a 1.6-fold excess of COS2 above substrate is required for 50% inhibition of RB-COS2 transport, whereas a 10.5-fold excess is required to inhibit RB-COS3 transport by the same amount. These data are compatible with the 6.9-fold lower apparent K_{uptake} of RB-COS3. Di-*N*-acetylchitobiitol (COS2ol) and GlcNAc do not inhibit LOST-mediated [^{3}H]M5 transport into lysosomes as efficiently as COS2 (Saint-Pol et al. 1999), and are 10–20-fold, and 100–200-fold, respectively, less effective at blocking RB-COS2 and RB-COS3 transport than COS2. As shown for [^{3}H]M5 transport (Fig. 3B), GlcNAc(Fuc)GlcNAc and $GlcNAc_2$-P are poor RB-COS/3 transport inhibitors (Fig. 7C). Similarly, whereas COS2-4 block [^{3}H]M5 transport (Saint-Pol et al JBC 1999) and RBCOS/3 transports (Fig. 7C) with similar efficiency, COS5/6 are less effective at inhibiting the transport of [^{3}H]M5 transport (Fig. 1B) and RB-COS/3 transport (Fig. 7C). As was found for [^{3}H]M5 transport (Fig. 3B), $ManGlcNAc_2$ is a more potent RB-COS/3 transport competitor than COS2. However, whereas [^{3}H]M5 transport is blocked equally efficiently by COS2 and $Man_3GlcNAc_2$ (Fig. 3B), RB-COS2/3 transport

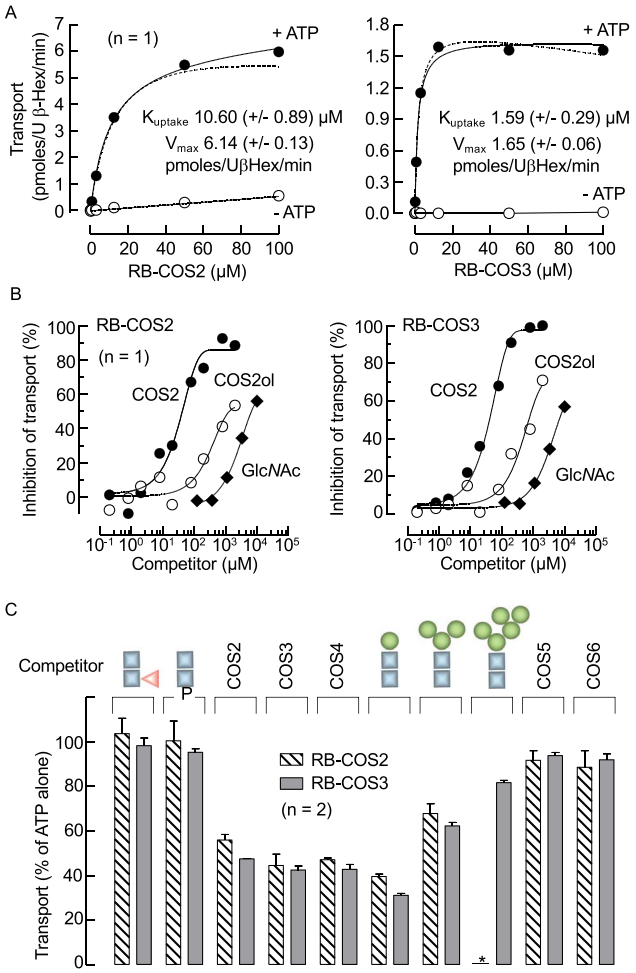

Fig. 7. Characteristics of RB-COS/3 transport into lysosomes. A) Apparent kinetic parameters for RB-COS2 and RB-COS3 transport into lysosomes were obtained by conducting transport assays with increasing amounts of substrate. After measuring the amount of β-Hex present in the incubations and generation of standard curves for probe fluorescence in L-meM/SH lysis buffer, the apparent transport constants K_{uptake} and V_{max} (+/−SD) were calculated using the GraphPad prism 5 Michaelis-Menten analysis of the ATP-dependent transport data sets (dotted lines). B) Transport assays using 20 μM RB-COS2 and 4 μM RB-COS3 were conducted in the presence of increasing quantities of COS2, di-N-acetylchitobiitol (COS2ol) and GlcNAc. The data are expressed as the % inhibition of ATP-dependent transport seen in the absence of competitor. C) Transport assays with 20 μM RB-COS2 and 4 μM RB-COS3 were conducted in the presence of the indicated competitors at a concentration of 40 μM. The asterisk indicates that $Man_5GlcNAc_2$ quenching of RB-COS2 transport was not performed.

is blocked somewhat less potently by $Man_3GlcNAc_2$ than by COS2 (Fig. 7B). Nevertheless, taken together, these data further substantiate the similar selectivities of RB-COS2/3 and [^{3}H]M5 transport processes.

[^{3}H]M5 and RB-COS transports are inhibited by bafilomycin and orthovanadate

To compare the biochemical properties of RB-COS2/3 and [^{3}H]M5 transports in more detail, their ATP dependencies were investigated. Transport into lysosomes could require the proton or voltage gradients across the lysosomal membrane that are generated by the bafilomycin A1-sensitive vacuolar ATPase (Fig. 8A), or could, for example, depend upon a

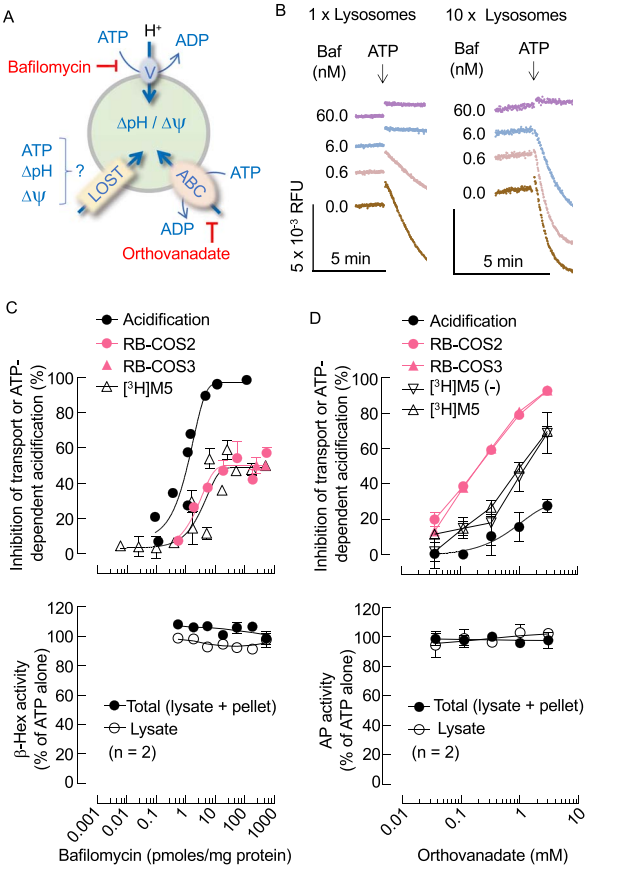

Fig. 8. The effects of bafilomycin and orthovanadate on [^{3}H]M5 and RB-COS2/3 transport into lysosomes. A) The electrogenic vacuolar proton pumping ATPase (V) is required for lysosomal acidification (ΔpH) and maintains a lysosomal membrane potential ($\Delta\psi$). Orthovanadate inhibits P-type ATPases such as ABC transporters at concentrations that do not inhibit the vacuolar ATPase. B) ATP-provoked lysosomal acidification was monitored by measuring the quenching (downward deflection) of acridine orange fluorescence as described in materials and methods. Bafilomycin (to give the indicated final concentrations) or its carrier DMSO were added 2 min prior to the addition of ATP. The traces on the right were obtained using 10-fold more of the lysosomal preparation. C) The inhibition of ATP-provoked lysosomal acidification, [^{3}H]M5 and RB-COS2/3 transports by bafilomycin are reported. Standard [^{3}H]M5, RB-COS2 (20 μM) and RB-COS3 (8 μM) transport assays, were conducted with known amounts of lysosomal protein in the presence of increasing amounts of bafilomycin, expressed as pmoles/mg lysosomal protein ($n = 2$). The inhibition of ATP-provoked lysosomal acidification was measured with different amounts of lysosomal protein using acridine orange quenching ($n = 1$). All data sets were treated using GraphPad prism 5 (Log_{10} agonist vs response, 4 parameters). The effect of bafilomycin on both L-meM mediated lysosomal rupture and lysosomal integrity during the RB-COS2 transport incubations was assessed by measuring the β-hexosaminidase (β-Hex) activities in the L-meM lysate and summing the β-Hex activities in the L-meM lysate and pellet to give the total activity recovered after the transport incubation. In both cases, the effect of bafilomycin is expressed as a percentage of values determined for incubations in the presence of ATP alone. D) The effect of orthovanadate on ATP-provoked lysosomal acidification as well as the standard [^{3}H]M5, RB-COS2 (20 μM) and RB-COS3 (8 μM) transport assays was studied ($n = 2$). Lysosomal acidification was measured in the presence of 5 mM ATP. In one experiment [^{3}H]M5 transport was measured in the presence of 5 mM ATP without the ATP regenerating system ([^{3}H]M5 (-)). The effect of orthovanadate on both L-meM mediated lysosomal rupture and lysosomal integrity during the RB-COS2 transport incubations was assessed as described above except that acid phosphatase (AP) was used as reporter activity.

process that directly couples transport with ATP hydrolysis as occurs with ATP-binding cassette (ABC)-type transporters, which are P-type ATPases that are inhibited by orthovanadate (IC_{50} 5–20 μM) (Fig. 8A). As previously reported (Bowman et al. 1988), and as shown in Fig. 8B, inhibition of lysosomal acidification by bafilomycin is dependent upon the quantity of the lysosomal preparation used. When employed in quantities of greater than 10 pmoles/mg lysosomal protein (Fig. 8C, upper panel), bafilomycin abolishes ATP-provoked lysosomal acidification while inhibiting RB-COS2/3 and [^{3}H]M5 transports maximally by 50% (Fig. 8C, upper panel). At these levels, bafilomycin has little affect upon either lysosomal stability during the transport incubation or, in the fluorescence assays, the amount of hydrolase released from the washed sedimentable material upon lysosomal rupture with L-meM (Fig. 8C, lower panel). Data in the upper panel of Fig. 8D show that RB-COS2/3 and [^{3}H]M5 transports are inhibited 50% by 0.25 and 1.0 mM sodium orthovanadate, respectively. These concentrations are 10–20-fold higher than those required to block typical ABC transporters and reduced (27% inhibition at 3 mM orthovanadate) ATP-provoked lysosomal acidification (Fig. 8D, upper panel). Although creatine kinase is not thought to be inhibited by vanadate ions (Boyd et al. 1985), [^{3}H]M5 transport assays were conducted in either the presence of 5 mM ATP alone or 5 mM ATP with the standard ATP regenerating system that includes creatine kinase. Despite the ATP regenerating system increasing [^{3}H]M5 transport 2.3-fold that seen in the presence of ATP alone in this experiment (data not shown), the orthovanadate inhibition curves are similar, confirming that the effect of orthovanadate is not through creatine kinase inhibition. Finally, orthovanadate did not affect lysosomal stability during transport incubations or the amount of hydrolase released from pelleted material upon lysosomal rupture with L-meM (Fig. 8D, lower panel).

Discussion

Transport of [^{3}H]COS2/4 into lysosomes

Before embarking on chemical modification of COS to generate fluorescent transport probes, it was necessary to find out if COS themselves are transported by LOST. The data presented in Figs 1–3 suggest that this is the case and that [^{3}H]COS2 and [^{3}H]COS4 transports display apparent $K_{uptakes}$ that are ~12- and ~8-fold, respectively, lower than that reported for [^{3}H]M5 (Saint-Pol et al. 1999). The previously determined apparent V_{max} for [^{3}H]M5 (7.1 pmoles/U β-Hex/min – reported as 7.1 fmoles/U β-Hex/min because 1 U of β-Hex was defined as 1 nmole PNP-GlcNAc hydrolyzed per min rather than the more common 1 μmole PNP-GlcNAc hydrolyzed per min used here) is 19- and 23-fold higher than the values obtained respectively for [^{3}H]COS2 and [^{3}H]COS3 transports. However, the apparent kinetic data obtained for [^{3}H]COS transport into lysosomes is of limited value because measurement of sedimentable GlcNAc as a workable proxy for COS2/4 import depends upon complete trapping of GlcNAc in the lysosome. This is not the case because in the presence of 300 μM CytB, GlcNAc is still apparent in the incubation medium. Furthermore, at this CytB concentration, LOST is also partially inhibited.

Although the physiological significance of the capacity of the lysosome to import COS is unknown, cytosolic COS are potentially generated during Hyaluronan (HA) biosynthesis. Some prokaryotic hyaluronan synthases (HAS) require a UDP-$GlcNAc_4$ primer (Weigel et al. 2015; Weigel et al. 2017) and under conditions where there is insufficient UDP-GlcA for HA biosynthesis, the UDP-$GlcNAc_4$ primer and free COS4 are detected (Weigel et al. 2015; Weigel et al. 2017). Whether or not mammalian HAS require such a primer is not clear, nevertheless several authors have suggested that COS generated in this way might have signaling functions during invertebrate and vertebrate development (Semino et al. 1996; Weigel et al. 2015; Weigel et al. 2017). Lysosomal import of COS could potentially regulate such signals. Of note, COS4 and COS5 are about 22 and 29 nm in length, respectively, which is similar to the thickness of a lipid bilayer and it has been suggested that the COS4 tetrasaccharide moiety at the start of each HA chain may help initiate passage of the nascent negatively charged HA chain through the cell membrane (Hascall 2019).

Transport of RB-COS2/3 into lysosomes

RB is weakly basic and potentially lysosomotropic. Nevertheless, it has been reported that rhodamine 123 (pKa 7.2) and rhodamine 6G (pKa 7.5) are not lysosomotropic, and it is thought that the delocalized charge on rhodamine dyes causes protonated and non-protonated forms to have similar lipid partitioning characteristics (Duvvuri et al. 2004). Presumably therefore, transport of RB-COS2/3 into lysosomes is measurable because the dye is not released from the sugar within the lysosome. In fact, our data indicate that whereas RB-COS3 is converted to RB-COS2 within lysosomes, RB-COS2 is quite stable.

All the synthetic fluorescent probes were shown to inhibit [^{3}H]M5 transport, and in the absence of the PEG2 spacer, inhibition potency increases as a function of COS length. This tendency is not apparent when the spacer is inserted between the sugar and fluorophore. Despite RB-COS4 being a more potent [^{3}H]M5 transport inhibitor than RB-COS2/3, the ATP-dependent RB-COS4 transport signal was low and could not be completely quenched with high concentrations of COS2. The placement of the PEG2 spacer between the sugar and RB moiety lowered the IC_{50} values for inhibition of [^{3}H]M5 transport, but strikingly reduced the ATP-dependent transport signal for RB-COS2 and RB-COS3. Although the low transport signals for probes with spacers is difficult to interpret, it is possible that these compounds, as well as RB-COS4, all have low K_{uptake} and V_{max} values, giving them inhibitor-like characteristics.

Are [^{3}H]M5, [^{3}H]COS and RB-COS2/3 transported by the same mechanism?

The final proof that one transport system is responsible for lysosomal import of fOS, COS and RB-COS2/3 will only be possible after identification of the underlying protein(s)/gene(s) and expression of the transport proteins an artificial membrane system. Data presented here do show that the [^{3}H]M5, [^{3}H]COS2/4, and RB-COS2/3 transport processes reveal similar sensitivities to a range of sugar based competitors (Figs 3B and 7C). [^{3}H]M5 and RB-COS2/3 transports are similarly sensitive to bafilomycin and orthovanadate (Fig. 8). It was previously reported (Saint-Pol et al. 1999) that 100 nM concanamycin A (a vacuolar ATPase inhibitor similar to bafilomycin A1) did not significantly inhibit LOST and it was concluded that the vacuolar ATPase was not required for ATP-dependent [^{3}H]M5 transport because this concanamycin A concentration is over 10-fold higher than that used to inhibit the vacuolar ATPase inhibitor in cells (Woo et al. 1992). However, because concanamycin A has a high affinity for

the vacuolar ATPase and the fOS transport assay requires relatively large amounts of lysosomes, it is possible that even higher amounts of this agent were needed to effectively block ATP driven acidification under the experimental conditions used (Saint-Pol et al. 1999). When the quantity of bafilomycin present in the different assays is expressed as pmoles/mg protein, it becomes apparent that inhibition of ATP-dependent [^{3}H]M5 transport is partially inhibited by drug doses similar to those required to inhibit lysosomal ATP-dependent acidification. Accordingly, although the possibility that bafilomycin blocks the transport processes independently of its inhibition of the vacuolar ATPase cannot be excluded, it can be speculated that the oligosaccharide transport processes require ATP hydrolysis independently of the vacuolar ATPase but are more efficient when the vacuolar ATPase is functioning. Whatever the mechanism of oligosaccharide transport inhibition by bafilomycin, it is apparent that the transport of [^{3}H]M5 and RB-COS2/3 are affected similarly. Both ATP-dependent [^{3}H]M5 and RB-COS2/3 transports are inhibited by orthovanadate. Generally, P-type ATPases and ABC transporters in particular are inhibited in the submicromolar to 20 μM concentration range (Cantley et al. 1978; Decottignies et al. 1998; Rao 1998), whereas the vacuolar ATPase is not inhibited by 0.1–0.5 mM concentrations of this agent (Moriyama et al. 1982; Ohkuma et al. 1982). Data reported here show weak inhibition of lysosomal acidification at 0.3–1.0 mM orthovanadate, but this cannot explain the striking inhibition of both [^{3}H]M5 and RB-COS2/3 transports seen over the same concentration range. The transport of the fluorescent probes appears more sensitive to orthovanadate than that of [^{3}H]M5. The origin of this difference remains to be determined, but the efficacy of inhibition of certain ABC transporters by vanadate is known to be dependent upon both the nature and concentration of the substrate that is being transported (Rao 1998).

In summary, we report the transport of [^{3}H]COS2, [^{3}H]COS4 and RB-COS analogs into lysosomes *in vitro*. The biochemical characteristics of these transports are similar to those of LOST-mediated [^{3}H]M5 transport, suggesting that the same, or closely related, mechanism underlies all of these transport processes. Our data show that lysosomal oligosaccharide import is not restricted to polymannose-type oligosaccharides and suggests that this process may play diverse roles in sugar metabolism. Finally, the data provide proof of concept for the use of COS modified at their non-reducing terminus as probes to study lysosomal oligosaccharide transport.

Materials and methods

Materials

[2-^{3}H]mannose (20 Ci/mmol), [^{3}H]GlcNAcβ1-4GlcNAc ([^{3}H]COS2, 1.6 Ci/mmol) and [^{3}H]GlcNAcβ1-4GlcNAcβ1-4GlcNAcβ1-4GlcNAc ([^{3}H]COS4, 1 Ci/mmol) were from BIOTREND (Hannover, DE). GlcNAcβ1-4GlcNAc-1P (COS2-1P) was synthesized as previously described (Bosco et al. 2017). GlcNAcβ1-4GlcNAcitol (COS2ol) was synthesized as described below. (GlcNAcβ1-4)$_{1\text{-}5}$GlcNAc (COS2-6), GlcNAcβ(1-4)(Fucα(1-6))GlcNAc, Manβ1-4GlcNAcβ1-4GlcNAc (ManGlcNAc$_2$), Manα1-3(Manα1-6)Manβ1-4GlcNAcβ1-4GlcNAc (Man$_3$*GlcNAc*$_2$), Manα1-6(Manα1-3)Manα1-6(Manα1-3)Manβ1-4GlcNAcβ1-4GlcNAc (Man$_5$GlcNAc$_2$), GlcNAcβ1-2Manα1-3(GlcNAcβ1-2Manα1-6)Manβ1-4GlcNAcβ1-4GlcNAc (GlcNAc$_2$Man$_3$GlcNAc$_2$); Dextra Laboratories (Reading, UK), AG™ 1-X2 (acetate form); Bio-Rad (Marnes-la-Coquette, FR), Ultima Gold and Ultima-Flo M; PerkinElmer (Villebon-sur-Yvette, FR), cell culture reagents; ThermoFisher Scientific (Villebon-sur-Yvette, FR). Rhodamine B isothiocyanate (RBITC) was purchased from Aldrich (lot: MKCJ0832). All other reagents and materials were from Merck (Darmstadt, DE).

Synthesis of chitooligosaccharide-based fluorescent probes and COS2ol

The de-*N*-acetylated COS2-4 (Chambon et al. 2017) were prepared from COS2-4 by treatment with *Sinorhizobium meliloti* NodB chitinoligosaccharide *N*-deacetylase in 20 mM MOPS pH 7.2 (Fig. 4A). They were isolated in 50% to 84% yield. The RB-PEG2-isothiocyanate **5** was synthetized from the commercially available PEG2 over 5 steps (Fig. 4B). The activation of both alcohol functions of PEG2 by mesyl chloride in the presence of triethylamine led to the dimesylate **1** and the subsequent substitution of both mesylates by sodium azide in DMF provided the diazide **2**. The selective reduction of a single azide under Staudinger conditions, i.e. in the presence of triphenyl phosphine and 1 M aqueous HCl in a THF/ether mixture, gave the azido-PEG2-amine **3**. The coupling of this amine **3** with RBITC in DMSO gave the corresponding RB-PEG2-azide **4**. Finally, the desired RB-PEG2-isothiocyanate **5** was obtained in the presence of triphenyl phosphine and carbon disulfide in anhydrous THF. The synthesis of the COS-based fluorescent probes was carried out by condensation of the de-*N*-acetylated COS2-4 with the appropriate isothiocyanate, i.e. either the commercially available rhodamine B isothiocyanate (RBITC) or the synthesized reagent **5** (Fig. 4C). They were isolated in yields ranging from 19% to 45%.

Finally, di-N-acetylchitobiitol (COS2ol) was prepared from per-acetylated COS2 prepared as described (Bosco et al. 2017). Deprotection of the acetate in anomeric position by potassium carbonate in methanol was followed by reduction with sodium borohydride in methanol and acetylation with acetic anhydride in pyridine. Total deprotection of acetates by sodium methylate in methanol then gave COS2ol in 84% yield.

Cell culture

The DPM1-deficient, mouse lymphoma Thy^{-1} cell line (Chapman et al. 1979; Trowbridge and Hyman 1979) ATCC, Rockville, MD) was cultivated in RPM1 1640 medium supplemented with 10% fetal bovine serum (FBS) in an atmosphere containing 5% CO_2.

Preparation of radioactive polymannose-type oligosaccharides

[^{3}H]Man$_{5\text{-}1}$GlcNAc were recovered from metabolically radiolabeled DPM1-deficient, mouse lymphoma Thy^{-1} cells (Chapman et al. 1979; Saint-Pol et al. 1999). After washing into the radiolabeling medium (glucose-free RPMI 1640 containing 10 nM concanamycin A, 10 mM HEPES, 2 mM glutamine, 1 mM pyruvate, 2 mM fucose and 5% dialyzed FBS) and resuspension at 20 $\times$ 10^6 cells/mL in the same medium, the cells were incubated for 4 h in the presence of 0.1 mCi/mL [2-^{3}H]mannose in a humidified incubator containing 5% CO_2. The cells were then harvested and rinsed twice with ice-cold phosphate buffered saline (PBS).

The cell pellets were suspended in 2 mL 100 mM Tris HCl (pH 7.4) containing 4 mM $MgCl_2$, 4 mL MeOH and 6 mL $CHCl_3$ and shaken vigorously. After separation of the phases by centrifugation, the upper aqueous/methanolic phase was recovered and dried under vacuum. The residue was resuspended in H_2O and loaded onto coupled columns (2 mL settled beads) of AmberChrom™ 50WX2 (H^+ form) and AG™ 1-X2 (acetate form) and the eluate and water washes were pooled and passed over columns of charcoal. After washing with H_2O, oligosaccharides were eluted with 30% EtOH to yield the [^{3}H]$Glc_{3\text{-}1}Man_{5\text{-}1}$GlcNAc preparation used in the standard LOST assay. A typical $Glc_{3\text{-}1}$[^{3}H]$Man_{5\text{-}1}$GlcNAc preparation comprises: 6.2% [^{3}H]Glc_3Man_5GlcNAc, 6.2% [^{3}H]Glc_2Man_5GlcNAc, 5.4% [^{3}H]Glc_1Man_5GlcNAc, 63.9% [^{3}H]Man_5GlcNAc, 14.1% [^{3}H]Man_4GlcNAc, 3.2% [^{3}H]Man_3GlcNAc, 0.6% [^{3}H]Man_2GlcNAc, 0.4% [^{3}H]Man_1GlcNAc. As [^{3}H]Man_5GlcNAc is the predominant species, this preparation is called [^{3}H]M5 throughout this report. Several batches of [^{3}H]M5 were used during this work and variability of the specific activities of these preparations may explain some differences in IC_{50} values determined for various competitors.

Preparation of rat liver lysosomes

Animals were housed and sacrificed in accordance with French government directives for the ethical use and treatment of animals for scientific purposes (Autorisation de Projet utilisant des Animaux à des Fins Scientifiques: APAFIS number 25276). Male or female Wistar rats (180–500 g) were starved for 14 h prior to being anaesthetized with isoflurane before liver removal and sacrifice. 8–10 g liver was finely minced with scissors at 4 °C. The liver pieces were suspended in 250 mM sucrose containing 10 mM HEPES and 1 mM EDTA, pH 7.3 (SHE) and after decantation the supernatant was discarded. This operation was repeated until the supernatant was clear. The liver pieces were then homogenized at 4 °C in 4 volumes of SHE with 18 plunges of the loose-fitting pestle in a Dounce homogenizer. The homogenate was diluted 1:1 with SHE and centrifuged at 900 g for 15 min at 4 °C. Both the supernatant and the pellet (after resuspension to 30 mL SHE) were recentrifuged as above and the resulting supernatants were pooled and made up to 130 mL with SHE and centrifuged (8 × 16 mL) at 23,286 g for 20 min at 4 °C. The combined pellets were resuspended to a total volume of 100 mL with SHE and mixed with 100 mL 80% Percoll (80 mL Percoll + 20 mL 5 × SHE). After centrifugation (8 × 24 mL) at 121,879 g for 45 min at 4 °C, the brown band containing the lysosomes, just above a clear Percoll-rich zone at the bottom of the tube, was collected. The lysosomal material was made up to 128 mL with 250 mM sucrose containing 10 mM HEPES, pH 7.3 (SH) and centrifuged (8 × 16 mL) at 23,286 g for 20 min at 4 °C. After removal of the supernatant, lysosomal material at the bottom of the tube was collected and made up to 32 mL with SH and recentrifuged (2 × 16 mL) at 23,286 g for 20 min at 4 °C. The final lysosomal pellets were resuspended in a volume of 0.1 mL of SH/g liver.

Standard lysosomal transport assays using [^{3}H]M5 or [^{3}H]COS

[^{3}H]M5 (40–50,000 cpm) was dried under vacuum into 1.5 mL reaction tubes. To this, 5 μL of either H_2O or an ATP regenerating system (50 mM ATP (Na^+) pH 7.0, 100 mM phosphocreatine (Na^+) and 0.05 mg/mL creatine kinase) was added, followed by 5 μL H_2O or water-soluble test compounds. Then, 20 μL of incubation buffer containing 350 mM sucrose, 125 mM KCl, 25 mM $MgCl_2$ and 10 μM swainsonine (SW) in 10 mM HEPES, pH 7.3 (IB) was added, and finally after mixing, 20 μL of the lysosome preparation was added. After mixing and standing on ice for 10 min, the tubes were incubated at 25 °C for different times. Transport reactions were stopped by addition of 1 mL ice cold SH. After centrifugation at 16,000 g for 10 min at 4 °C and removal of the supernatant, the pellet was resuspended in 1 mL SH and recentrifuged as above to yield a final lysosomal pellet that was solubilized in 300 μL SH containing 0.5% NP-40. Aliquots of this material were assayed for radioactivity by scintillation counting or β-hexosaminidase (β-Hex) activity (Opheim and Touster 1977).

For transport assays using [^{3}H]chitooligosaccharides ([^{3}H]COS), reaction tubes containing 50,000 cpm ([^{3}H]COS2) or ([^{3}H]COS4) were supplemented exactly as described above except that the IB contained 750 μM cytochalasin B (CytB) instead of SW. After incubation for 20 min at 25 °C, the reaction mixtures were stopped by the addition of 0.5 mL SH containing 300 μM CytB. After centrifugation at 16,000 g for 10 min at 4 °C and removal of the supernatant, the pellet was resuspended in 0.5 mL SH/CytB and centrifuged as above to yield a final lysosomal pellet, which was processed as described for the [^{3}H]M5 transport assay. Technical duplicates were performed ($n = 2$) except in some experiments where several data points are used to generate best fit curves using GraphPad Prism 5, in which case $n = 1$.

Size exclusion chromatography of transport incubation mixtures

Where indicated, [^{3}H]COS2 transport assays conducted in the absence or presence of CytB were stopped by the addition of 300 μL H_2O and incubated at 100 °C for 5 min. After cooling, the tubes were centrifuged at 16,000 g for 10 min at 4 °C. The supernatants were loaded onto a 0.8 × 59 cm column of Biogel-P2 (fine) equilibrated with 100 mM acetic acid. In other experiments, the reactions were stopped by addition of 300 μL ice-cold SH (−/+ CytB) and after centrifugation the supernatant and the pellet (extracted as described for whole incubations) were loaded onto the column separately. The column was irrigated at a flow rate of 0.5 mL/min and 0.5 mL fractions were collected and monitored for radioactive components by scintillation counting. The column was calibrated using [^{3}H]COS2 and [^{3}H]GlcNAc.

Transport of fluorescent COS derivatives into lysosomes

COS-based fluorescent probes were incubated with lysosomes in the absence or presence of ATP and various competitors as described above in a final volume of 125 μL in 2.5 mL reaction tubes. For these assays, SW and CytB were omitted from the IB. Reactions were stopped by the addition of 1.8 mL ice cold SH. After centrifugation at 16,000 g for 10 min at 4 °C, the pellet was washed again. The final pellet was resuspended in 500 μL SH, and one 200 μL aliquot was transferred to a tube containing 200 μL 2.5 mM D-methyl methionine ester (D-meM) in SH and a second 200 μL aliquot transferred to another tube containing 200 μL 2.5 mM L-methyl methionine ester (L-meM) in SH. After incubating on

ice for 15 min, the tubes were centrifuged at 16,000 g for 10 min at 4 °C and the supernatants were removed, and fluorescence intensity was measured (Ex 520 nm/Em 580 nm) using a Tecan Spark microplate reader. Lysosomal rupture was monitored by measuring β-Hex and/or acid phosphatase (AP) activities (Opheim and Touster 1977). Generally, technical duplicates were performed as described for the assays using radioactive substrates.

Mass spectrometric analysis of fluorescent probe catabolism

For mass spectrometry of probes associated with lysosomal pellets after transport incubations, standard transport assays containing either no probe or 10 μM RB-COS3 were performed and stopped as described above. After centrifugation, aliquots of the supernatants were heated to 100 °C for 10 min, cooled, and made 1% with respect to formic acid. The transport pellets were washed again, and the L-meM lysates, prepared as described above, were heated at 100 °C for 10 min and treated as described for the supernatants. All samples were made up to 3 mL with 1% formic acid (FA) and loaded onto SepPak C18 cartridges preequilibrated with 1% FA. After washing with 4 mL 1% FA, and 4 mL each of 4%, 12%, and 20% AcN in 1% FA, the fluorescent probes were eluted with 4 mL each of 28% and 36% AcN in 1% FA. These fractions were pooled and dried under vacuum overnight. Samples were resuspended in 20 μL of 80% MeOH, 20% H_2O. For electrospray ionization high resolution mass spectrometry (ESI-HRMS), 1–5 μL were injected with a continuous infusion of methanol at 60 μL.min^{-1} into an LTQ-Orbitrap XL (Thermo Fisher Scientific, Courtaboeuf, France) operated in positive ionization mode, with a spray voltage at 3.6 kV and an ion transfer capillary temperature of 275 °C. Detection was achieved in the Orbitrap with a resolution of 100,000 (at m/z 400) and a m/z range between 150–2,000 in profile mode. The spectra were recorded using the acquisition software XCalibur 2.1 (Thermo Fisher Scientific, Courtaboeuf, France). Automatic gain control (AGC) was 2.10^5 ions, maximum injection time was 500 ms. Internal lockmass was enabled using in-house reference compounds.

Monitoring lysosomal acidification with acridine orange

The quenching of acridine orange fluorescence after movement into lysosomes was measured as previously reported (Moriyama et al. 1982). Fluorescence (Ex: 488 nm, Em 530 nm) was measured in plastic cuvettes containing 0.8 mL SH, 0.8 mL IB without SW or CytB, 20 μg/mL acridine orange, and 380 μL H_2O. This mixture was allowed to equilibrate in the fluorimeter (Photon Technology International QuantaMaster Spectrofluorometer) at 25 °C with stirring for 5 min before addition of lysosomes in SH. After stabilization of lysosome induced quenching, ATP was added to a final concentration of 1 or 5 mM to initiate vacuolar ATPase dependent acidification. Bafilomycin A1 or its carrier DMSO were added in a maximum volume of 5 μL 2 min prior to the addition of ATP.

Abbreviations

AcN; acetonitrile, AP; lysosomal acid phosphatase, COS; chitooligosaccharide, COS2ol; di-*N*-acetylchitobiitol, Ctbs; lysosomal chitobiase, CytB; cytochalasin B, FA; formic acid, fOS; free polymannose type oligosaccharide, HA; hyaluronan, HEPES; 4-(2-hydroxyethyl)-1-piperazineethanesulfonic acid, β-Hex; lysosomal β-hexosaminidase, LOST; lysosomal oligosaccharide transport, D-meM; D-methyl methionine ester, L-meM; L-methyl methionine ester, PUGNAc; *O*-(2-acetamido-2-deoxy-d-glucopyranosylidene)amino-*N*-phenylcarbamate, RB; rhodamine B, RBITC; rhodamine B isothiocyanate, SH; sucrose/HEPES buffer, SW; swainsonine.

Acknowledgements

P.B. and C.G-P. gratefully acknowledge the assistance of P. Gerardo (Université Paris Cité) for low-resolution and high-resolution mass spectra analyses and the NMR platform core facilities of the BioTechMed facilities INSERM US36 | CNRS UMS2009 | Université Paris Cité for NMR experiments. S.F. acknowledges the NanoBio ICMG (UAR 2607) for providing facilities for mass spectrometry (A. Durand, L. Fort, R. Gueret) and NMR analyses (I. Jeacomine).

Author contributions

Younès Bouzidi (Conceptualization [equal], Formal analysis [equal], Investigation [lead], Methodology [lead], Writing—original draft [equal], Writing—review & editing [equal]), Micheël Bosco (Conceptualization [lead], Formal analysis [equal], Investigation [lead], Methodology [lead], Supervision [equal], Writing—original draft [equal], Writing—review & editing [equal]), Haifei Gao (Conceptualization [lead], Data curation [equal], Formal analysis [equal], Investigation [lead], Methodology [lead], Writing—original draft [supporting], Writing—review & editing [supporting]), Stéphanie Pradeau (Formal analysis [equal], Investigation [equal], Methodology [equal], Project administration [equal], Writing—review & editing [equal]), Lucrèce Matheron (Conceptualization [equal], Data curation [equal], Formal analysis [equal], Investigation [equal], Methodology [equal], Validation [equal], Writing—review & editing [equal]), Isabelle Chantret (Conceptualization [supporting], Investigation [supporting], Methodology [equal], Project administration [equal], Supervision [supporting], Writing—original draft [supporting], Writing—review & editing [equal]), Sébastien Fort (Conceptualization [lead], Data curation [supporting], Formal analysis [equal], Funding acquisition [lead], Investigation [equal], Methodology [supporting], Project administration [lead], Resources [lead], Supervision [equal], Validation [equal], Writing—original draft [equal], Writing—review & editing [equal]), Patricia Busca (Conceptualization [lead], Data curation [equal], Formal analysis [equal], Funding acquisition [equal], Investigation [equal], Methodology [equal], Project administration [equal], Supervision [equal], Validation [equal], Writing—original draft [equal], Writing—review & editing [equal]), Christine Gravier-Pelletier (Conceptualization [lead], Formal analysis [equal], Funding acquisition [lead], Investigation [supporting], Methodology [equal], Project administration [lead], Supervision [equal], Validation [equal], Writing—original draft [lead], Writing—review & editing [equal]), and Stuart Moore (Conceptualization [lead], Data curation [equal], Formal analysis [equal], Funding acquisition [equal], Investigation [lead], Methodology [lead], Project administration [equal], Supervision [equal], Validation [equal], Writing—original draft [lead], Writing—review & editing [lead]).

Funding

This work was supported by the Fondation pour la Recherche Medical [DCM20181039551 to C.G-P.]; the French National Research Agency [ANR-18-CE44-0007 to S.M., ANR-17-EURE-0003 and ANR-15-IDEX-02 to S.F.]; Institut Carnot PolyNat [CARN-025-01 to S.F.] and institutional funding from INSERM and CNRS.

Conflict of interest statement: None declared.

References

Aronson NN, Halloran BA. Optimum substrate size and specific anomer requirements for the reducing-end glycoside hydrolase di-N-acetylchitobiase. Biosci Biotechnol Biochem. 2006:70(6): 1537–1541.

Aronson NNJ, Backes M, Kuranda MJ. Rat liver chitobiase: purification, properties, and role in the lysosomal degradation of Asn-linked glycoproteins. *Arch Biochem Biophys*. 1989:**272**(2):290–300.

Bosco M, Massarweh A, Iatmanen-Harbi S, Bouhss A, Chantret I, Busca P, Moore SEH, Gravier-Pelletier C. Synthesis and biological evaluation of chemical tools for the study of dolichol linked oligosaccharide diphosphatase (DLODP). *Eur J Med Chem*. 2017:**125**:952–964.

Bowman EJ, Siebers A, Altendorf K. Bafilomycins: a class of inhibitors of membrane ATPases from microorganisms, animal cells, and plant cells. *Proc Natl Acad Sci U S A*. 1988:**85**(21):7972–7976 accessed 2022 May 14.

Boyd DW, Kustin K, Niwa M. Do vanadate polyanions inhibit phosphotransferase enzymes? *Biochim Biophys Acta*. 1985:**827**(3):472–475.

Cantley LCJ, Cantley LG, Josephson L. A characterization of vanadate interactions with the (Na,K)-ATPase. Mechanistic and regulatory implications. *J Biol Chem*. 1978:**253**(20):7361–7368.

Chambon R, Pradeau S, Fort S, Cottaz S, Armand S. High yield production of rhizobium NodB chitin deacetylase and its use for in vitro synthesis of lipo-chitinoligosaccharide precursors. *Carbohydr Res*. 2017:**442**:25–30.

Chantret I, Fasseu M, Zaoui K, Le Bizec C, Sadou Yayé H, Dupré T, Moore SEH. Identification of roles for peptide: N-glycanase and endo-beta-N-acetylglucosaminidase (Engase1p) during protein N-glycosylation in human HepG2 cells. *PLoS One*. 2010:**5**(7):e11734.

Chapman A, Trowbridge IS, Hyman R, Kornfeld S. Structure of the lipid-linked oligosaccharides that accumulate in class E Thy-1-negative mutant lymphomas. *Cell*. 1979:**17**(3):509–515.

Codogno P, Mehrpour M, Proikas-Cezanne T. Canonical and non-canonical autophagy: variations on a common theme of self-eating? *Nat Rev Mol Cell Biol*. 2011:**13**(1):7–12.

Decottignies A, Grant AM, Nichols JW, de Wet H, McIntosh DB, Goffeau A. ATPase and multidrug transport activities of the over-expressed yeast ABC protein Yor1p. *J Biol Chem*. 1998:**273**(20): 12612–12622.

Demirel O, Bangert I, Tampé R, Abele R. Tuning the cellular trafficking of the lysosomal peptide transporter TAPL by its N-terminal domain. *Traffic*. 2010:**11**(3):383–393.

Demirel Ö, Jan I, Wolters D, Blanz J, Saftig P, Tampé R, Abele R. The lysosomal polypeptide transporter TAPL is stabilized by interaction with LAMP-1 and LAMP-2. *J Cell Sci*. 2012:**125**(Pt 18):4230–4240.

Duvvuri M, Gong Y, Chatterji D, Krise JP. Weak base permeability characteristics influence the intracellular sequestration site in the multidrug-resistant human leukemic cell line HL-60. *J Biol Chem*. 2004:**279**(31):32367–32372.

van Eijk M, van Roomen CPAA, Renkema GH, Bussink AP, Andrews L, Blommaart EFC, Sugar A, Verhoeven AJ, Boot RG, Aerts JMFG. Characterization of human phagocyte-derived chitotriosidase, a component of innate immunity. *Int Immunol*. 2005:**17**(11): 1505–1512.

Goldman R. Ion distribution and membrane permeability in lysosomal suspensions. *Front Biol*. 1976:**45**:309–336.

Hascall VC. The journey of hyaluronan research in the journal of biological chemistry. *J Biol Chem*. 2019:**294**(5):1690–1696.

Hase K, Contu VR, Kabuta C, Sakai R, Takahashi M, Kataoka N, Hakuno F, Takahashi S-I, Fujiwara Y, Wada K, et al. Cytosolic domain of SIDT2 carries an arginine-rich motif that binds to RNA/DNA and is important for the direct transport of nucleic acids into lysosomes. *Autophagy*. 2020:**16**(11):1974–1988.

Iwai K, Mega T, Hase S. Detection of $Man_5GlcNAc$ and related free oligomannosides in the cytosol fraction of hen oviduct. *J Biochem*. 1999:**125**(1):70–74.

Jonas AJ, Jobe H. *N*-acetyl-D-glucosamine countertransport in lysosomal membrane vesicles. *Biochem J*. 1990:**268**(1):41–45.

Jonas AJ, Speller RJ, Conrad PB, Dubinsky WP. Transport of N-acetyl-D-glucosamine and N-acetyl-D-galactosamine by rat liver lysosomes. *J Biol Chem*. 1989:**264**(9):4953–4956.

Kaushik S, Cuervo AM. The coming of age of chaperone-mediated autophagy. *Nat Rev Mol Cell Biol*. 2018:**19**(6):365–381.

Kimura M, Umeyama T, Wakita S, Okawa K, Sakaguchi M, Matoska V, Bauer PO, Oyama F. Direct comparison of chitinolytic properties and determination of combinatory effects of mouse chitotriosidase and acidic mammalian chitinase. *Int J Biol Macromol*. 2019:**134**: 882–890.

Macauley MS, Vocadlo DJ. Increasing O-GlcNAc levels: an overview of small-molecule inhibitors of O-GlcNAcase. *Biochim Biophys Acta*. 2010:**1800**(2):107–121.

Moore SEH. Oligosaccharide transport: pumping waste from the ER into lysosomes. *Trends Cell Biol*. 1999:**9**(11):441–446.

Moriyama Y, Takano T, Ohkuma S. Acridine orange as a fluorescent probe for lysosomal proton pump. *J Biochem*. 1982:**92**(4): 1333–1336.

Ohashi S, Iwai K, Mega T, Hase S. Quantitation and isomeric structure analysis of free oligosaccharides present in the cytosol fraction of mouse liver: detection of a free disialobiantennary oligosaccharide and glucosylated oligomannosides. *J Biochem*. 1999:**126**(5): 852–858.

Ohkuma S, Moriyama Y, Takano T. Identification and characterization of a proton pump on lysosomes by fluorescein-isothiocyanate-dextran fluorescence. *Proc Natl Acad Sci U S A*. 1982:**79**(9): 2758–2762.

Opheim DJ, Touster O. The purification and characterization of rat liver lysosomal alpha-L-fucosidase. *J Biol Chem*. 1977:**252**(2):739–743.

Persichetti E, Klein K, Paciotti S, Lecointe K, Balducci C, Franken S, Duvet S, Matzner U, Roberti R, Hartmann D, et al. Lysosomal di-N-acetylchitobiase-deficient mouse tissues accumulate Man2GlcNAc2 and Man3GlcNAc2. *Biochim Biophys Acta*. 2012:**1822**(7):1137–1146.

Pierce RJ, Spik G, Montreuil J. Cytosolic location of an endo-N-acetyl-beta-D-glucosaminidase activity in rat liver and kidney. *Biochem J*. 1979:**180**(3):673–676.

Rao US. Drug binding and nucleotide hydrolyzability are essential requirements in the vanadate-induced inhibition of the human P-glycoprotein ATPase. *Biochemistry*. 1998:**37**(42):14981–14988.

Reeves JP. Accumulation of amino acids by lysosomes incubated with amino acid methyl esters. *J Biol Chem*. 1979:**254**(18): 8914–8921.

Reeves JP, Reames T. ATP stimulates amino acid accumulation by lysosomes incubated with amino acid methyl esters. Evidence for a lysosomal proton pump. *J Biol Chem*. 1981:**256**(12): 6047–6053.

Saint-Pol A, Bauvy C, Codogno P, Moore SEH. Transfer of free polymannose-type oligosaccharides from the cytosol to lysosomes in cultured human hepatocellular carcinoma HepG2 cells. *J Cell Biol*. 1997:**136**(1):45–59.

Saint-Pol A, Codogno P, Moore SEH. Cytosol-to-lysosome transport of free polymannose-type oligosaccharides. Kinetic and specificity studies using rat liver lysosomes. *J Biol Chem*. 1999:**274**(19): 13547–13555.

Semino CE, Specht CA, Raimondi A, Robbins PW. Homologs of the Xenopus developmental gene DG42 are present in zebrafish and mouse and are involved in the synthesis of Nod-like chitin oligosaccharides during early embryogenesis. *Proc Natl Acad Sci U S A*. 1996:**93**(10):4548–4553.

Suzuki T, Yano K, Sugimoto S, Kitajima K, Lennarz WJ, Inoue S, Inoue Y, Emori Y. Endo-beta-N-acetylglucosaminidase, an enzyme involved in processing of free oligosaccharides in the cytosol. *Proc Natl Acad Sci U S A*. 2002:**99**(15):9691–9696.

Suzuki T, Hara I, Nakano M, Shigeta M, Nakagawa T, Kondo A, Funakoshi Y, Taniguchi N. Man2C1, an alpha-mannosidase, is involved in the trimming of free oligosaccharides in the cytosol. *Biochem J*. 2006:**400**(1):33–41.

Trowbridge IS, Hyman R. Abnormal lipid-linked oligosaccharides in class E Thy^{-1}-negative mutant lymphomas. *Cell*. 1979:**17**(3): 503–508.

Verbert A, Cacan R. Trafficking of oligomannosides released during N-glycosylation: a clearing mechanism of the rough endoplasmic reticulum. *Biochim Biophys Acta*. 1999:**1473**(1):137–146.

Weigel PH, West CM, Zhao P, Wells L, Baggenstoss BA, Washburn JL. Hyaluronan synthase assembles chitin oligomers with -GlcNAc(α1→)UDP at the reducing end. *Glycobiology*. 2015:**25**(6):632–643.

Weigel PH, Baggenstoss BA, Washburn JL. Hyaluronan synthase assembles hyaluronan on a [GlcNAc(β1,4)]n-GlcNAc(α1→)UDP primer and hyaluronan retains this residual chitin oligomer as a cap at the nonreducing end. *Glycobiology*. 2017:**27**(6):536–554.

Woo J-T, Shinohara C, Sakai K, Hasumi K, Endo A. Isolation, characterization and biological activities of concanamycins as inhibitors of lysosomal acidification. *J Antibiot*. 1992:**45**(7):1108–1116.

Yanagida K, Natsuka S, Hase S. Structural diversity of cytosolic free oligosaccharides in the human hepatoma cell line, HepG2. *Glycobiology*. 2006:**16**(4):294–304.